Redox Biology 30 (2020) 101437

Contents lists available at ScienceDirect

Redox Biology

journal homepage: www.elsevier.com/locate/redox

Comparative analysis of the mitochondrial morphology, energy metabolism, and gene expression signatures in three types of blastocyst-derived stem cells

Joonhyuk Choi[a,1], Bong Jong Seo[a,1], Hyeonwoo La[a], Sang Hoon Yoon[a], Yean Ju Hong[a], Ji-Heon Lee[b], Hyung-Min Chung[b], Kwonho Hong[a], Jeong Tae Do[a,*]

[a] Department of Stem Cell and Regenerative Biotechnology, Konkuk Institute of Technology, Konkuk University, Seoul, Republic of Korea
[b] Department of Stem Cell Biology, School of Medicine, Konkuk University, Seoul, Republic of Korea

ARTICLE INFO

Keywords:
Embryonic stem cells (ESCs)
Trophoblast stem cells (TSCs)
Extraembryonic endoderm stem cells (XEN cells)
Mitochondria
Metabolism

ABSTRACT

Pre-implantation mouse blastocyst-derived stem cells, namely embryonic stem cells (ESCs), trophoblast stem cells (TSCs), and extraembryonic endoderm (XEN) cells, have their own characteristics and lineage specificity. So far, several studies have attempted to identify these three stem cell types based on genetic markers, morphologies, and factors involved in maintaining cell self-renewal. In this study, we focused on characterizing the three stem cell types derived from mouse blastocysts by observing cellular organelles, especially the mitochondria, and analyzing how mitochondrial dynamics relates to the energy metabolism in each cell type. Our study revealed that XEN cells have distinct mitochondrial morphology and energy metabolism compared with that in ESCs and TSCs. In addition, by analyzing the energy metabolism (oxygen consumption and extracellular acidification rates), we demonstrated that differences in the mitochondria affect the cellular metabolism in the stem cells. RNA sequencing analysis showed that although ESCs are developmentally closer to XEN cells in origin, their gene expression pattern is relatively closer to that of TSCs. Notably, mitochondria-, mitochondrial metabolism-, transport/secretory action-associated genes were differentially expressed in XEN cells compared with that in ESCs and TSCs, and this feature corresponds with the morphology of the cells.

1. Introduction

Late blastocyst of mouse consists of three types of cell lineages including pluripotent epiblast, primitive endoderm (PrE), and trophectoderm (TE) [1]. These three lineage cell types show specific directions of differentiation: epiblast gives rise to all cell types of a body, PrE to parietal and visceral yolk sac, and TE to placenta. These lineage-specific cell types can be cultured *in vitro* and be established as stem cells, such as embryonic stem cells (ESCs) from epiblast [2], extraembryonic endoderm (XEN) cells from PrE [3], and trophoblast stem cells (TSCs) from TE [4]. These stem cells share two fundamental characteristics, namely self-renewal and differentiation potential, which vary depending on the type of stem cells. ESCs can differentiate into all embryonic cell types making up the whole body and germ cells [5]. However, XEN cells and TSCs cannot contribute to embryonic tissue, but can differentiate into the PrE lineage and trophoblast lineage, respectively [4,6].

Over the past decades, researchers have investigated the energy metabolism in early mammalian embryo and preimplantation embryo-derived stem cells [7,8]. Energy, or adenosine-5′-triphosphate (ATP), production through mitochondrial oxidative phosphorylation (OXPHOS) allows cells to efficiently produce energy using oxygen [9]. Generally, cells containing mature form of mitochondria are known to use OXPHOS for energy production [10]. However, exceptional cases have been observed in early embryo-derived stem cells. The ESCs derived from early stage epiblast in blastocyst have immature form of mitochondria, while the epiblast stem cells (EpiSCs) derived from late stage epiblast in implanted embryos have relatively mature form of mitochondria [11]. Zhou et al. reported that EpiSCs utilize anaerobic glycolysis exclusively, while ESCs utilize glycolysis and OXPHOS for energy production [11]. Metabolizing glycolysis under normoxic condition, called aerobic glycolysis or the Warburg effect, was first discovered in cancer cells [12,13]. Moreover, studies regarding mitochondrial dynamics have also focused on whether the mitochondria

* Corresponding author. Tel.: 82 2 450 3673; fax: 82 2 455 1044.
E-mail address: dojt@konkuk.ac.kr (J.T. Do).
[1] These authors contributed equally to this work.

https://doi.org/10.1016/j.redox.2020.101437
Received 4 November 2019; Received in revised form 16 January 2020; Accepted 17 January 2020
Available online 20 January 2020

can affect cellular fate [14]. Therefore, further studies are needed to define the differences and characteristic of the three stem cell types (ESCs, XEN cells, and TSCs) derived *in vitro* from different cell lineages in preimplantation embryos (epiblast, PrE, and TE), and more details are needed to verify the extent of differences between these three stem cell types. However, there has been no detailed study on the morphology and metabolism of mitochondria in both TSC and XEN cells, although the mitochondrial morphology in ESCs was previously reported [15]. Since it is known that self-renewal and differentiation potential of stem cells are correlated with the metabolic state and the culture environment [16], we attempted to identify the differences that may exist between ESCs, TSCs, and XEN.

Here, we established ESC, TSC, and XEN cell lines from cultured blastocysts and compared their mitochondrial morphologies, energy metabolism, and gene expression profiles. A detailed mitochondrial and metabolic profile of these stem cells would provide the basic properties of these three cell types and could clarify some of the vague aspects of these three stem cell types. Furthermore, the bioenergetic data could provide novel insights into the mitochondrial dynamics and metabolic change during early embryo development.

2. Materials & methods

2.1. Cell lines establishment and culture

Extraembryonic endoderm stem (XEN) cells, embryonic stem cells (ESCs), and trophoblast stem cells (TSCs) were derived from blastocysts cultured on a dish with G-2 plus (Vitrolife, 10132, Sweden) covered with Ovoil (Vitrolife, 10029). Then, the blastocysts were attached to a dish layered with inactivated mouse embryonic fibroblasts (MEFs) in the mouse ES medium, consisting of Dulbecco's modified Eagle's medium (D-MEM) low glucose (Hyclone, 11885-084, GE Healthcare, Melbourne, VIC, Australia) supplemented with 15% heat-inactivated fetal bovine serum (Hyclone), 1× penicillin/streptomycin/glutamine (Gibco, 10378-016, Grand Island, NY, USA), 0.1 mM nonessential amino acids (Gibco, 11140-050), 1 mM β-mercaptoethanol (Gibco, 21985-023), and 10^3 U/mL leukemia inhibitory factor (ESGRO, Merck Millipore), for establishment of XEN cells and ESCs, and in the TSC medium, consisting of Rosewell Park Memorial Institute (RPMI) 1640 medium (Gibco, 11875-093) supplemented with 20% heat-inactivated fetal bovine serum (Hyclone), 1× penicillin/streptomycin/glutamine (P/S/G; Gibco, 10378-016), 1mM of β-mercaptoethanol (Gibco, 21985-023), Human recombinant FGF4 (25 ng/ml) (Sigma, F8424, St. Louis, MO, USA) and heparin (1 μg/ml), for establishment of TSCs. Stem cells derivation from the blastocysts were closely observed through a microscope on defined conditions. When a distinct morphology of a specific stem cell was observable, the cells were passaged on to a new MEFs layered dishes and the media were changed to the culture medium. ESCs and TSCs were maintained over 20 passages in mouse ES, TSC medium, respectively. XEN cells were maintained over 20 passages in XEN medium, consisting of RPMI 1640 medium (Gibco) supplemented with 15% heat-inactivated fetal bovine serum (Hyclone), 1× P/S/G (Gibco), 1mM of β-mercaptoethanol (Gibco).

2.2. RNA isolation and qRT-PCR

RNA extraction was carried out by using TRIzol reagent (Invitrogen, 15596026, Carlsbad, CA, USA) according to standard protocols. cDNA was synthesized from 1 μg of total RNA using SuperScript III Master Mix (Enzynomics, RT300S, Daejeon, Republic of Korea) according to the manufacturer's instructions. Real-time polymerase chain reaction (real-time PCR) was performed with TOPreal™ qPCR 2X PreMIX (Enzynomics, RT500 M), and results were analyzed on a Roche LightCycler 5480 (Roche, Swiss). Thermal cycling was carried out via 45 cycles of 10 s at 95 °C, 10 s at 60 °C, and 20 s at 72 °C. The primers for real-time PCR are shown in Table 1.

2.3. Immunocytochemistry

For the immunocytochemistry, the cells were cultured on 4-well dishes until 70–80% confluency. The cells were fixed with 4% paraformaldehyde for 10 min at 4 °C and then washed with PBS and treated with 0.3% triton X-100 in PBS for 10 min. After then, the cells were blocked with PBS containing 3% bovine serum albumin and 0.3% triton X-100 for 1 h at 25 °C (room temperature). The blocked cells were then incubated overnight at 4 °C with the following primary antibodies: Oct4 (1:500; Santa Cruz Biotechnology), Nanog (1:500; Abcam, ab80892, Cambridge, UK), Gata4 (1:200; Abcam, ab84593), SOX17 (1:300; R&D systems, AF1924, Minneapolis, MN, USA). The following day, incubated cells were washed with PBS for 10 min three times and incubated with fluorescently labeled (Alexa Fluor 488 or 568; Abcam) secondary antibodies. The secondary antibodies were used according to the manufacturer's specifications. The cells were lastly washed and stained with DAPI in 0.3% triton X-100 in PBS for 2 min at 25 °C.

2.4. Electron microscopy

For transmission electron microscope (TEM) observations, the samples were fixed in 4% paraformaldehyde (Sigma) and 2.5% glutaraldehyde (Sigma) in 0.1 M phosphate (Sigma) buffer overnight. After washing in 0.1 M phosphate buffer, the samples were post-fixed for 1 h in 1% osmium tetroxide (Sigma) prepared in the same buffer. The samples were dehydrated with a graded series of ethyl alcohol concentrations, embedded in Epon 812, and polymerized at 60 °C for 3 days. Ultrathin sections (60–70 nm) were obtained using an ultramicrotome (Leica Ultracut UCT, Germany). Ultrathin sections collected on grids (200 mesh) were examined in TEM (JEM 1010) operating at 60 kV, and images were recorded by a charge-coupled device camera (SC1000; Gatan).

2.5. Mitochondrial length analysis

The images from electron microscopy were analyzed and measured by the Image J 1.43 (NIH) software for calculating the maximum (Max)/minimum (Min) ratio of mitochondrial length. At least over fifty mitochondria were measured and analyzed per sample to obtain data.

2.6. Oxygen consumption rate analysis

For measuring oxygen consumption rate (OCR), we used Seahorse extracellular flux (XF96) analyzer. In all, total 1×10^4 cells of ESCs, XEN cells, and TSCs were attached in XF96 Cell Culture Microplate precoated with Matrigel in mES, XEN, TSC medium, respectively, before 24 h from the assay. After a medium change to XF base media supplemented D-glucose (1g/L, Sigma, G8769), Sodium pyruvate (1 mM, Gibco, 11360-070) and L-glutamine (4 mM, Gibco, 25030-081), the assay was performed by using XF96 Extracellular Flux Analyzers (Seahorse Bioscience, North Billerica, MA, USA). Four measurements were obtained under basal conditions and after the addition of several chemicals such as oligomycin (1 μM), FCCP (1 μM) and rotenone (1 μM)/antimycin A (1 μM) (Agilent Technologies, 103015-100, Santa Clara, CA, USA). The process after treatment was performed following the manufacturer's instructions.

2.7. Extracellular acidification rate analysis

To measure the extracellular acidification rate (ECAR), we used a Seahorse extracellular flux (XF96) analyzer. In all, a total of 1.5×10^4 ESCs, XEN cells, and TSCs were cultured in XF96 Cell Culture Microplate pre-coated with Matrigel in mES, XEN, TSC medium, respectively, 24 h prior to the assay. After a medium change to XF base media supplemented L-glutamine (4 mM, Gibco, 25030-081), the assay was performed using XF96 Extracellular Flux Analyzers (Seahorse

Table 1
Primer sets used for real-time PCR.

	Forward	Reverse
GAPDH	5′-GGCAAATTCAACGGCACAGT-3′	5′-GTCTCGCTCCTGGAAGATGG-3′
Pou5f1	5′-GGCTTCAGACTTCGCCTTCT-3′	5′-TGGAAGCTTAGCCAGGTTCG-3′
Nanog	5′-CAGGTGTTTGAGGGTAGCT-3′	5′-CGGTTCATCATGGTACAGTC-3′
Gata6	5′-ACCATCACCCGACCTACTCG-3′	5′-CGACAGGTCCTCCAACAGGT-3′
Pdgfra	5′-CCTCAGCGAGATAGTGGAGAAC-3′	5′-ACCGATGTACGCATTATCAGAGT-3′
Dab2	5′-GGCAACAGGCTGAACCATTAGT-3′	5′-TTGGTGTCGATTTCAGAGTTTAGAT-3′
Tead4	5′- TCTGGGCAGACCTCAATACC-3′	5′-CCAAATGAGCAGACCTTCGT-3′
Cdx2	5′-ATTGTTTGCTGCTGTTCGAGTC-3′	5′-CGACTTCCCTTCACCATACAAC-3′

Bioscience, North Billerica, MA, USA). Four measurements were obtained under basal conditions and after the addition of several chemicals such as D-glucose (10 mM), oligomycin (1 μM), and 2-Deoxy-D-glucose (50 mM) (Agilent Technologies, 103020-100). The process after treatment was performed according to the manufacturer's instructions.

2.8. Direct measurement of adenosine triphosphate level

To measure the adenosine triphosphate (ATP) levels, we used a luminescent ATP detection assay kit (Abcam, ab113849) with GloMax 96 Microplate Luminometer (Promega, E6521, Madison, WI, USA). A total of 1×10^4 ESCs, XEN cells, and TSCs were cultured in 96 well cell culture plates (SPL life science, 30296, Gyeonggi-do, Korea) pre-coated with Matrigel in mES, XEN, TSC medium, respectively, 24 h prior to the assay. The process after treatment was performed according to the manufacturer's instructions.

2.9. RNA sequencing

Total RNA samples were converted into cDNA libraries using the TruSeq Stranded mRNA Sample Prep Kit (Illumina). Starting with 100 ng of total RNA, polyadenylated RNA (mainly mRNA) was selected and purified using oligo dT-conjugated magnetic beads. This mRNA was physically fragmented and converted into single-stranded cDNA using reverse transcriptase and random hexamer primers, with the addition of Actinomycin D to suppress DNA-dependent synthesis of the second strand. Double-stranded cDNA was created by removing the RNA template and synthesizing the second strand in the presence of dUTP (deoxy-ribo-uridine triphosphate) in place of dTTP (deoxythymidine triphosphate). A single A base was added to the 3¢ end to facilitate ligation of sequencing adapters, which contain a single T base overhang. Adapter-ligated cDNA was amplified by polymerase chain reaction to increase the amount of sequence-ready library. During this amplification, the polymerase stalls when it encounters a U base, rendering the second strand a poor template. Accordingly, the amplified material used the first strand as a template, thereby preserving the strand information. Final cDNA libraries were analyzed for size distribution and using an Agilent Bioanalyzer (DNA 1000 kit; Agilent), quantitated by qPCR (Kapa Library Quant Kit; Kapa Biosystems, Wilmington, MA, USA), then normalized to 2 nM in preparation for sequencing.

2.10. Sequenced read processing

Validity of sequenced reads were accessed with FastQC (v0.11.5) and the reads were aligned with STAR (v2.5.2b) to UCSC mouse mm10 genome assembly. StringTie (v1.3.3b) was used to process STAR results into transcript assemblies. Results from StringTie were used to calculate average expression of each gene in FPKM and the acquired values were used for drawing scatter plots in R (v3.6.1). For heatmaps, FPKM value of individual samples and heatmap2 function of R's gplots (v3.0.1.1) package were used. In all cases, DEGs were identified with aforementioned cutoff value using calculations with R. With the resulting DEGs from scatter plot and heatmap, gene ontology and KEGG pathway analysis were conducted through DAVID (v6.8).

2.11. Statistical analysis

All experiments in this study were reproduced with independent samples derived from different embryos. All experiments were performed in triplicate and data represented as means ± standard deviation of the mean (SD). The significance of differences was assessed by student's *t*-test or one-way analysis of variance (ANOVA) with Tukey Honestly Significant Difference (HSD) host hoc for multiple comparisons. p-values < 0.05 were considered statistically significant.

2.12. Animal use ethical statement

All methods used in this study were carried out in accordance with national animal care and use guidelines laws, and all experimental protocols were approved by the Institutional Animal Care and Use Committee of Konkuk University.

3. Result

3.1. In vitro establishment of three types of stem cells from blastocyst

ESCs, TSCs, and XEN cells, can be derived from preimplantation blastocysts [17]. We tried to derive new ESCs, TSCs, and XEN cell lines from the same mouse strain. First, 2-cell stage embryos were collected from 1.5 dpc (days post coitum) B6D2F1 female mouse mated through hormonal induction of superovulation. The embryos were cultured *in vitro* until they reached the late blastocyst stage (Fig. 1A). Each blastocyst was then transferred to separate feeder-layered dishes with different culture conditions for ESCs, TSCs, and XEN cells. Each stem cell line was continuously passaged under the cell type-specific culture conditions until distinctive cell morphology was observable within a single well. Through this, we were able to establish three distinct stem cell lines derived from the same strain blastocysts (Fig. 1B). ESCs formed dome-like morphology of colonies (Fig. 1B, top), while TSCs formed flat colonies with clear boundaries (Fig. 1B, bottom). The XEN cells were small cobblestone shaped and formed flat colonies in which the boundary between cells were easily distinguishable (Fig. 1B, middle). In addition, we compared cell proliferation rate of these three cell types by counting the cell number during the maintenance of each stem cell line (Fig. 1C). ESCs showed the highest proliferation rate among the three cell types, while XEN cells showed the lowest proliferation rate.

3.2. Characterization of three different stem cells derived from blastocyst

After confirming the morphological characteristics, we investigated molecular characteristics of the three different stem cell types by immunocytochemistry analysis using specific markers (Fig. 2A–C). ESCs stained positive for core pluripotency markers Oct4 and Nanog (Fig. 2A), and TSCs stained positive for Eomes (Fig. 2B). We observed

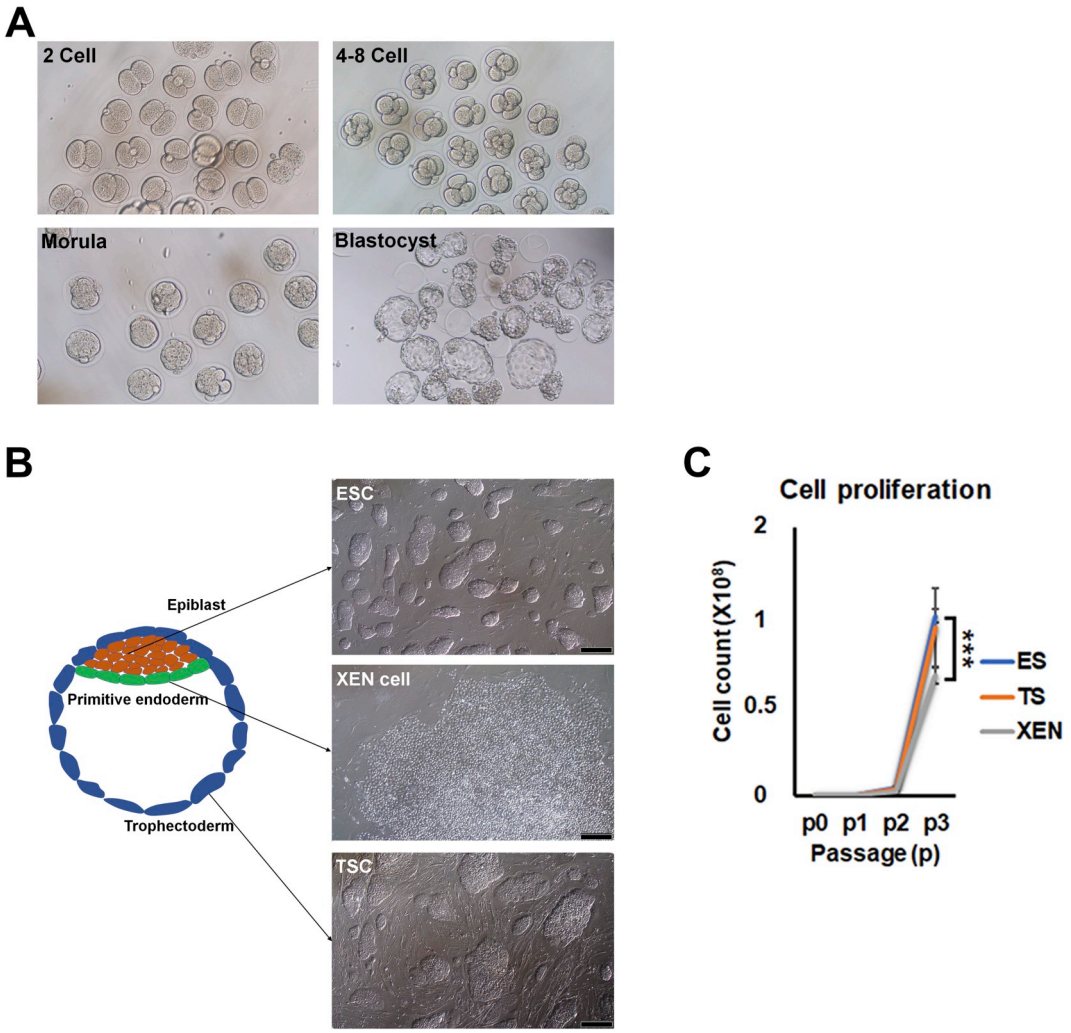

Fig. 1. Derivation of embryo origin stem cells in defined conditions. (A) Representative images of embryos cultured from 2-cell stage (1.5 dpc, left side) to blastocysts (3.5–4.5 dpc, right side). Scale bars: 200 μm **(B)** Representative images of established stem cells derived from embryos using defined conditions. ESCs from epiblast (top), TSCs from trophectoderm (bottom) and XEN cells from primitive endoderm (middle). Scale bars: 200 μm. Student's *t*-test: ***$p < 0.001$.

the primitive endoderm markers, Gata4 and Sox17, in the established XEN cells (Fig. 2C). Due to uncertainties regarding the markers that were used in the immunocytochemical analysis, we proceeded with quantitative real-time RT-PCR to characterize these stem cells more thoroughly. ESCs overexpressed Oct4 and Nanog compared to XEN cells (Fig. 2D). TSCs overexpressed TE markers, Tead4 and Cdx2 (Fig. 2E) compared to ESCs (Fig. 2. E). XEN cells were shown to express noticeably high levels of Dab2, Gata6, and Pdgfra in contrast to ESCs (Fig. 2F), These results confirmed that the three distinct cell types were properly established from the blastocysts.

3.3. Mitochondrial morphologies in the three blastocyst-derived stem cell types

As the three blastocyst-derived stem cell types represent three distinct lineages of early embryo, and thus showed distinct characteristics, we hypothesized that their intracellular ultrastructure might be different from that of each other. As a first approach to test this, we compared the intracellular organelles of each cell type by examining the morphology of nuclei and mitochondria in ESCs, TSCs, and XEN cells by using electron microscopy (Fig. 3A and B). It is known that pluripotent stem cells have larger nucleus to cytoplasm ratio than differentiated cells [15]; thus, we expected the pluripotent ESCs to show larger nucleus to cytoplasm ratio than the other two stem cell types. However, ESCs and TSCs showed similar nucleus to cytoplasm ratio, and both of them displayed a larger ratio than the XEN cells (Fig. 3A). Next, we checked mitochondrial morphology of the three stem cell types. Pluripotent ESCs showed globular-shaped mitochondria as expected. To our surprise, mitochondrial morphologies were also globular-shaped in the TSCs (Fig. 3B). In XEN cells, although they showed elongated rod-shaped mitochondria compared with those in the ESCs and TSCs, the lengths of the mitochondria were much shorter than that seen in differentiated somatic cells such as fibroblast [15] (Fig. 3B, Supplementary Fig. 1). Moreover, the mitochondria had immature cristae in ESCs and TSCs, while those in XEN cells were relatively well-developed (Fig. 3B). For the accurate measurement of mitochondrial morphologies, we measured the calculated-maximal (c-Max) and calculated-minimal (c-Min) axes' length of mitochondria in these stem cells (Fig. 3C–E). The mean values of the c-Max/c-Min ratio in ESCs and TSCs were 1.46 and 1.51, respectively, which were significantly lower than that in XEN cells (2.19) (Fig. 3D-E). In addition, we observed mitochondrial morphology of early stage embryo from oocyte to blastocyst (Supplementary Figs. 2A–F). Unfertilized oocyte, 2-, 4-cell embryos, and morula showed globular-shaped mitochondria (Supplementary Figs. 2A–D). Next, we compared the mitochondrial morphology of Inner Cell Mass (ICM) and TE cells of blastocyst (Supplementary Figs. 2E–H). To our surprise, we could not find any significant differences in mitochondrial morphology between these

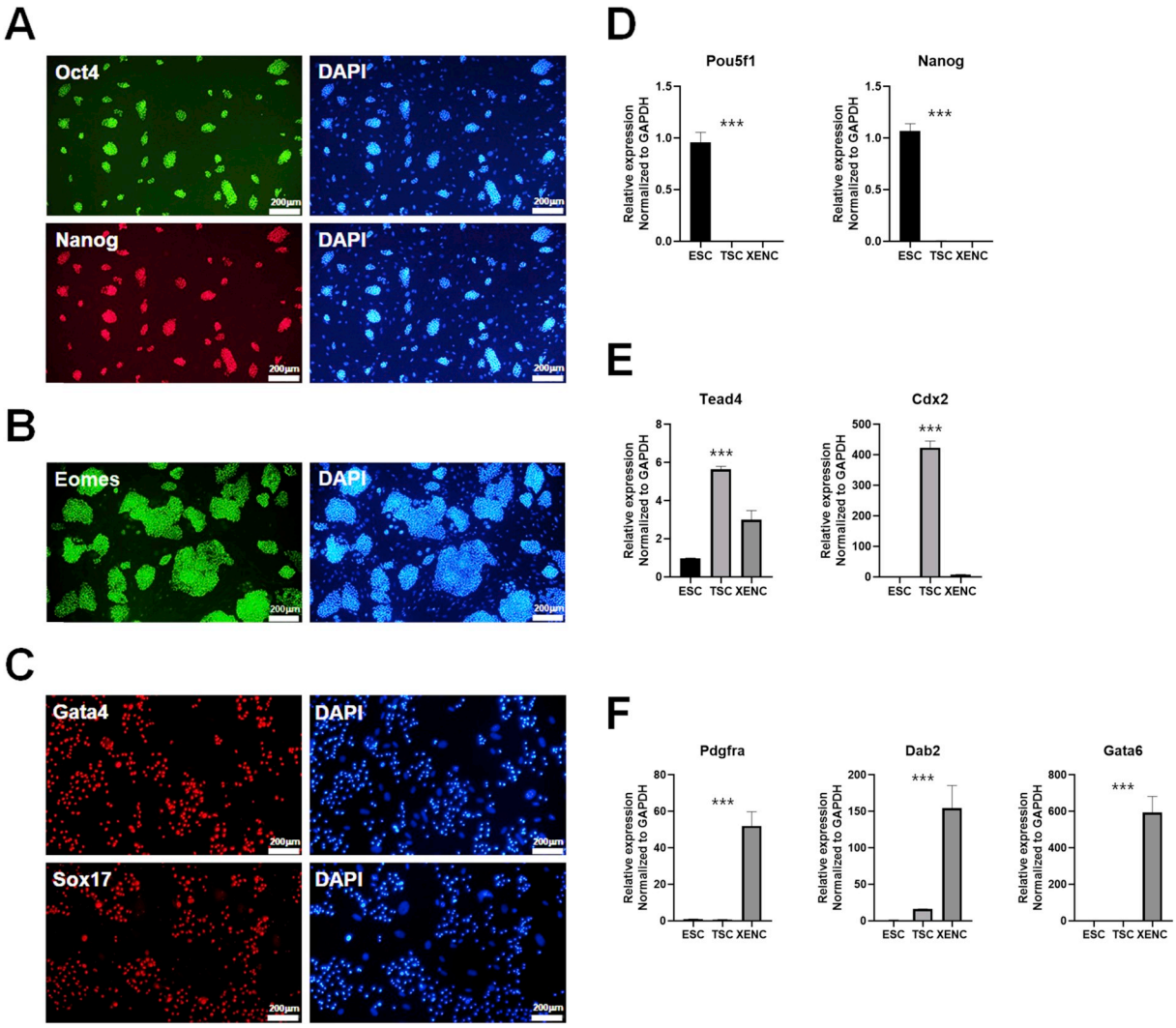

Fig. 2. Analysis of stem cell lineages established from blastocysts. **(A–C)** Immunocytochemical analysis of XEN cells, TSCs, and ESCs. Scale bars: 200 μm **(A)** XEN cells were immunoreactive to Gata4 (red) and Sox17 (red), known as the markers of primitive endoderm, proving the primitive endodermal lineage. Nuclei were stained with DAPI (blue). **(B)** TSCs were stained to observe expression of Eomes (green). **(C)** ESCs were shown to express pluripotent markers Oct4 (green) and Nanog (red). **(D–G)** qRT-PCR analysis of XEN cells, TSCs, and ESCs. Data are presented as mean ± SEM for n = 3 independent experiments. **(D)** Strong expression of Dab2, Gata6, and Pdgfra were observed in XEN cells compared with that in control ESC. **(E)** TSCs strongly expressed Tead4 and Cdx2, while pluripotency marker Pou5f1 expression was repressed compared to that in ESCs. **(F)** ESCs were analyzed with standard pluripotency marker Nanog. **(G)** Cell counting for comparing cell proliferation of blastocyst-derived stem cells. One-way ANOVA: ***$p < 0.001$. ESC, embryonic stem cells; TSC, trophoblast stem cells; XEN, extraembryonic endoderm. (For interpretation of the references to colour in this figure legend, the reader is referred to the Web version of this article).

cells. Collectively, the round shaped mitochondria of ICM and TE cells were maintained through *in vitro* establishment of ESCs and TSCs. Next, we observed other intracellular organelles such as the Golgi stack, endoplasmic reticulum (ER), endosomes, and lysosomes in these stem cells (Fig. 3A). We could not observe any differences in Golgi stack, endosomes, and lysosomes. Interestingly, however, ERs in XEN cells were relatively swollen compared with those in ESCs and TSCs (Fig. 5G).

3.4. Distinct energy metabolism in the three blastocyst-derived stem cell types

Cells constantly adjust energy metabolism in response to environmental changes and energy demands. Thus, main energy metabolism differs for each cell type. Many studies on energy metabolism have been conducted in pluripotent stem cells, but little has been studied in TSCs and XEN cells. Thus, we tried to compare energy metabolism in the three cell types, which showed distinct mitochondrial morphologies, by measuring the oxygen consumption rate (OCR), which represents the OXPHOS activity (Fig. 4A). Interestingly, the ESCs showed approximately three times higher level of basal respiration compared to the TSCs, although they have similar mitochondrial morphology (Fig. 4A and B). The XEN cells, which contained relatively more mature form of mitochondria than the ESCs and TSCs, showed basal respiration that was lower than that in the ESCs and higher than that in the TSCs (Fig. 4A-B). After treatment with oligomycin, an ATP synthase inhibitor, the OCR levels of all samples reduced to the basal level. Then each sample was treated with FCCP to measure the maximal respiration, including the spare capacity (Fig. 4A). FCCP is a mitochondrial uncoupling agent, which collapses the proton gradient by transporting protons across the mitochondrial inner membranes and disrupting the mitochondrial membrane potential. After FCCP treatment, the maximal respiration could be measured (Fig. 4A and C), which was dramatically increased in two XEN cell lines, but only slightly increased in ESCs and TSCs (Fig. 4A and C), indicating that XEN cells are more dependent on OXPHOS than ESCs and TSCs for energy production. In addition, unlike XEN cells, ESCs and TSCs showed little spare respiratory capacity (Fig. 4D). Furthermore, despite having immature form of mitochondria,

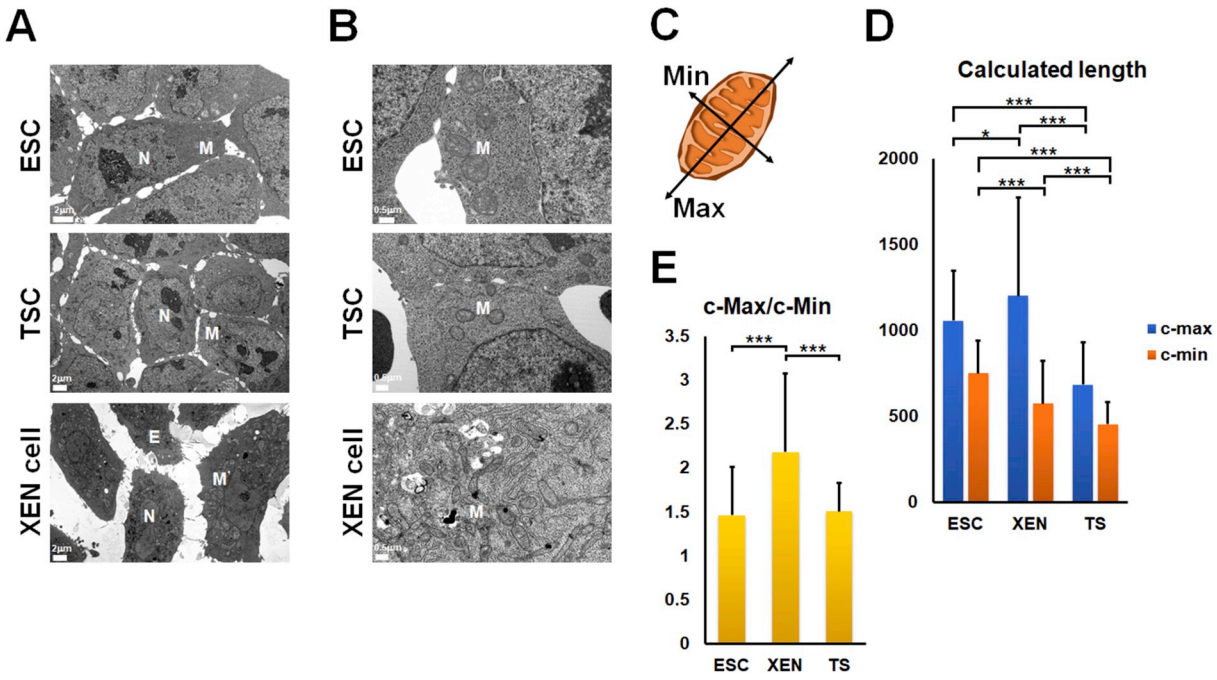

Fig. 3. Mitochondrial analysis of established stem cells. **(A)** Representative image of each stem cell observed through a transmission electron microscope (TEM). Nuclei (N), Endoplasmic reticulum (E), Mitochondria (M) and other organelles are observable. Scale bar: 2 μm **(B)** Enlarged TEM images of each stem cells focused on the mitochondria. Scale bar: 0.5 μm **(C)** Criteria used to analyze mitochondria morphological difference among the stem cells. **(D)** Quantitively analyzed mitochondrial length by using the criteria. **(E)** The ratio of c-Max and c-Min axes of mitochondria. Student's *t*-test: $*p < 0.05$, $**p < 0.01$, and $***p < 0.001$. ESC, embryonic stem cells; TSC, trophoblast stem cells; XEN, extraembryonic endoderm.

the ESCs showed the highest level of ATP-linked respiration among the three stem cell types, although the differences were not significant compared with that in XEN cells (Fig. 4E). Additionally, XF Cell Energy Phenotype analysis showed that XEN cells showed the most high energetic cell state response to oxygen stress (Fig. 4F). Next, we tried to compare extracellular acidification rate (ECAR), which represents the glycolytic activity (Supplement Figure. 3). Remarkably, TSCs showed higher level of glycolytic function including glycolysis, glycolytic capacity, and glycolytic reserve than did ESCs, although they showed similar mitochondrial morphology (Supplement Fig. 3A–D). The XEN cells, which contained relatively more mature forms of mitochondria than the ESCs, showed similar levels of glycolysis and glycolytic capacity (Supplement Fig. 3B-C). However, XEN cells exhibited a slightly lower level of glycolytic reserve than did the ESCs (Supplement Figure. 3D). Finally, we conducted an ATP level assay to measure the amount of ATP production in ESCs, TSCs, and XEN cells. Irrespective of OCR data, TSCs showed the higher ATP production levels than did the ESCs and XEN cells (Fig. 4G).

Taken together, these results demonstrate that the three blastocyst-derived stem cell types show have distinct energy metabolism characteristics, which can be partially interpreted based on mitochondrial morphology.

3.5. Global gene expression patterns in ESCs, TSCs, and XEN cells

Next, we performed RNA-seq analysis to compare the global gene expression patterns between ESCs, TSCs, and XEN cells. Our analysis revealed 4315, 4762, and 4002 genes to be differentially expressed in ESCs *vs.* TSCs, ESCs *vs.* XEN cells, and XEN cells *vs.* TSCs, respectively (FPKM $>$ 2, fold change $>$ 2) (Fig. 5A). Among the 4315 differentially expressed genes (DEGs), 2312 genes were more abundantly expressed in ESCs, whereas 2003 genes were more abundantly expressed in TSCs (Fig. 5A). Among the 4762 DEGs, 2377 and 2385 genes were more abundantly expressed in ESC and XEN cells, respectively. Among the 4002 DEGs, 2152 and 1850 genes were more abundantly expressed in XEN cells and TSCs, respectively (Fig. 5A).

Correlation matrix showed that the gene expression pattern in TSCs was more closer to that in ESCs than that in XEN cells (Fig. 5C), indicating that although ESCs are more developmentally closer to XEN cells in origin, the gene expression pattern is more closer to TSCs. Our analysis also identified pluripotency-, hypoblast-, and trophoblast-enriched genes (Fig. 5D). As expected, the pluripotency-related genes were found to be enriched in ESCs (Fig. 5D), the hypoblast-related genes were enriched in XEN cells, and the trophoblast-related genes were highly expressed in the TSCs (Fig. 5D). Additionally, we compared the expression of early developmental genes that we reported on previously [18] in ESCs, TSCs, and XEN cells (Supplementary Fig. 4). Each cell line had a distinct gene expression pattern in early developmental genes (Supplementary Fig. 4). The RNA-seq analysis verified that the three cell types displayed lineage-specific gene expression and distinct global gene expression patterns.

Next, we attempted to identify biological functions of the specific genes upregulated in ESCs, TSCs, and XEN cells (Fig. 5B). Gene ontology-biological process (GO:BP) analysis of ESCs showed that upregulated genes in ESCs were enriched in the terms ‘transcription’, ‘multicellular organism development’, and ‘cell cycle’ (Fig. 5B, red bars). The upregulated genes in TSCs were enriched in the terms ‘transforming growth factor beta receptor signaling pathway’, ‘cell migration’, and ‘apoptotic process’ (Fig. 5B, blue bars). Notably, GO:BP analysis of XEN cells showed that upregulated genes in XEN cells were enriched in the terms ‘protein transport’, ‘vesicle-mediated transport’, and ‘ER to Golgi vesicle-mediated transport’, suggesting that XEN cells might have paracrine effect on the adjacent cells (Fig. 5B, green bars).

Hierarchical clustering analysis of 5,050 DEGs revealed 6 clusters with unique signature: ESC-specific genes (clusters 1 and 6, downregulated and upregulated in ESCs, respectively), TSC-specific genes (clusters 2 and 4, upregulated and downregulated in TSCs, respectively), and XEN cell-specific genes (clusters 3 and 5, downregulated and upregulated in XEN cells, respectively) (Fig. 5E). To our surprise, GO:BP analysis of cluster 1 indicated that ESCs showed specific

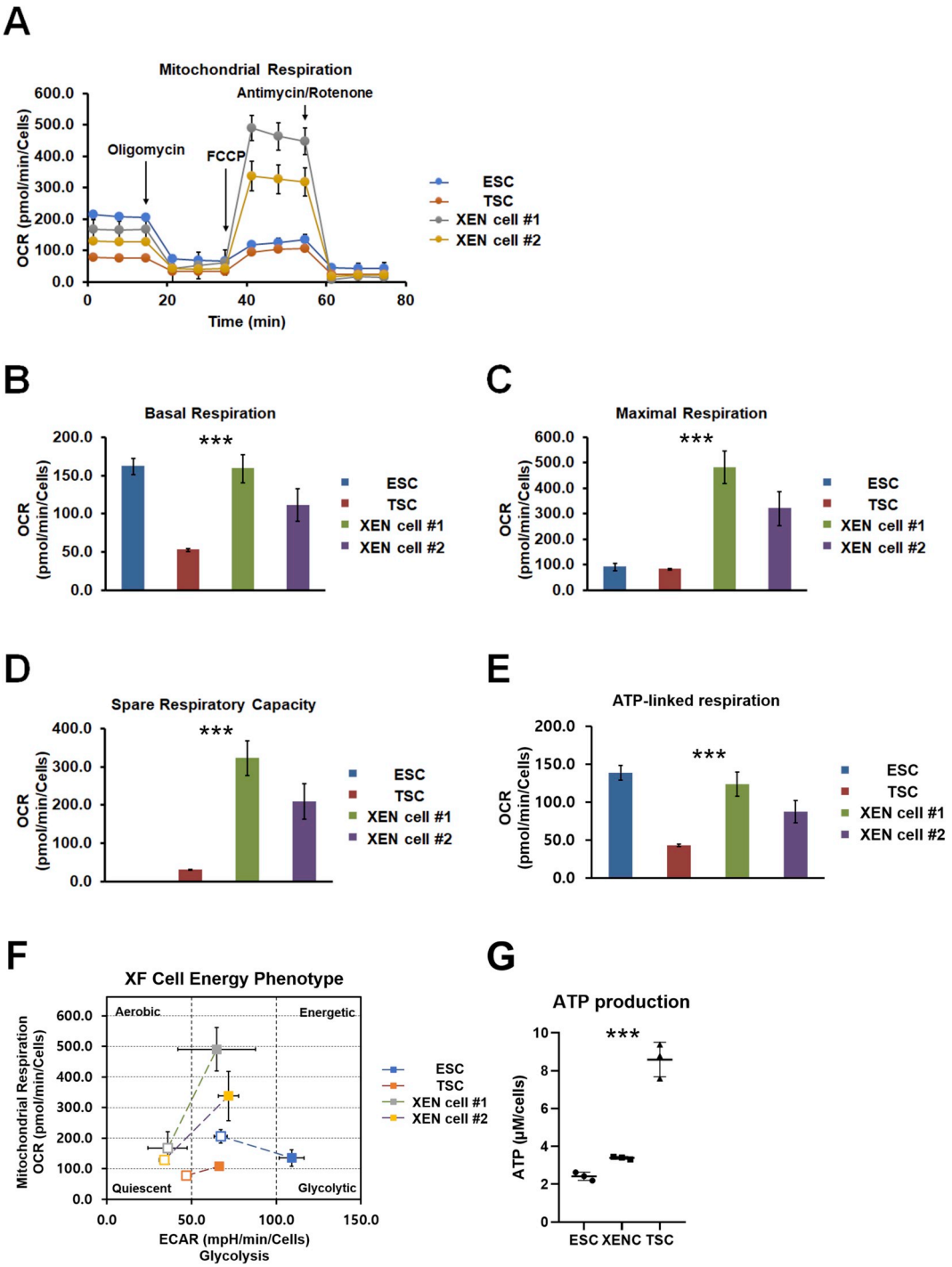

Fig. 4. Metabolic changes in blastocyst-derived stem cells. **(A)** Measurement of oxygen consumption rate (OCR) in ESC, TSC, and XEN cells. Measurement of **(B)** basal respiration, **(C)** maximal respiration, **(D)** spare respiratory capacity, and **(E)** ATP production in ESC, TSC, and XEN cells. **(F)** Measurement of energy phenotype in ESC, TSC, and XEN cells. The empty square shows the baseline of cell state. The filled square shows the cell state response to oxygen stress. **(G)** Direct measurement of ATP levels in ESC, TSC, and XEN cells. One-way ANOVA: $***p < 0.001$. ESC, embryonic stem cells; TSC, trophoblast stem cells; XEN, extraembryonic endoderm.

downregulation of genes related to transport such as 'protein transport', 'vesicle-mediated transport', and 'intracellular protein transport' (Supplementary Fig. 5). This could be because ESCs, which have relatively fast cell cycles, are likely to make full use of intracellularly synthesized proteins for their own cell division. In contrast, GO:BP analysis of cluster 5 revealed that XEN cells showed specific upregulation of genes related to transport such as 'vesicle-mediated transport', 'ER to Golgi vesicle-mediated transport', and 'protein transport' (Supplementary Fig. 5).

Next, we performed Kyoto encyclopedia of genes and genomes (KEGG) analysis to understand functions and utilities of the biological system (Supplementary Fig. 6). Interestingly, KEGG pathway of cluster 5 showed that XEN cells highly expressed genes involved in 'protein processing in endoplasmic reticulum' (Supplementary Fig. 6, orange). Taken together, these results indicate that XEN cells might show active protein transport or secretion, particularly in ERs.

To see if there are morphological differences involved in transport/secretory action observed only in XEN cells, we further observed the

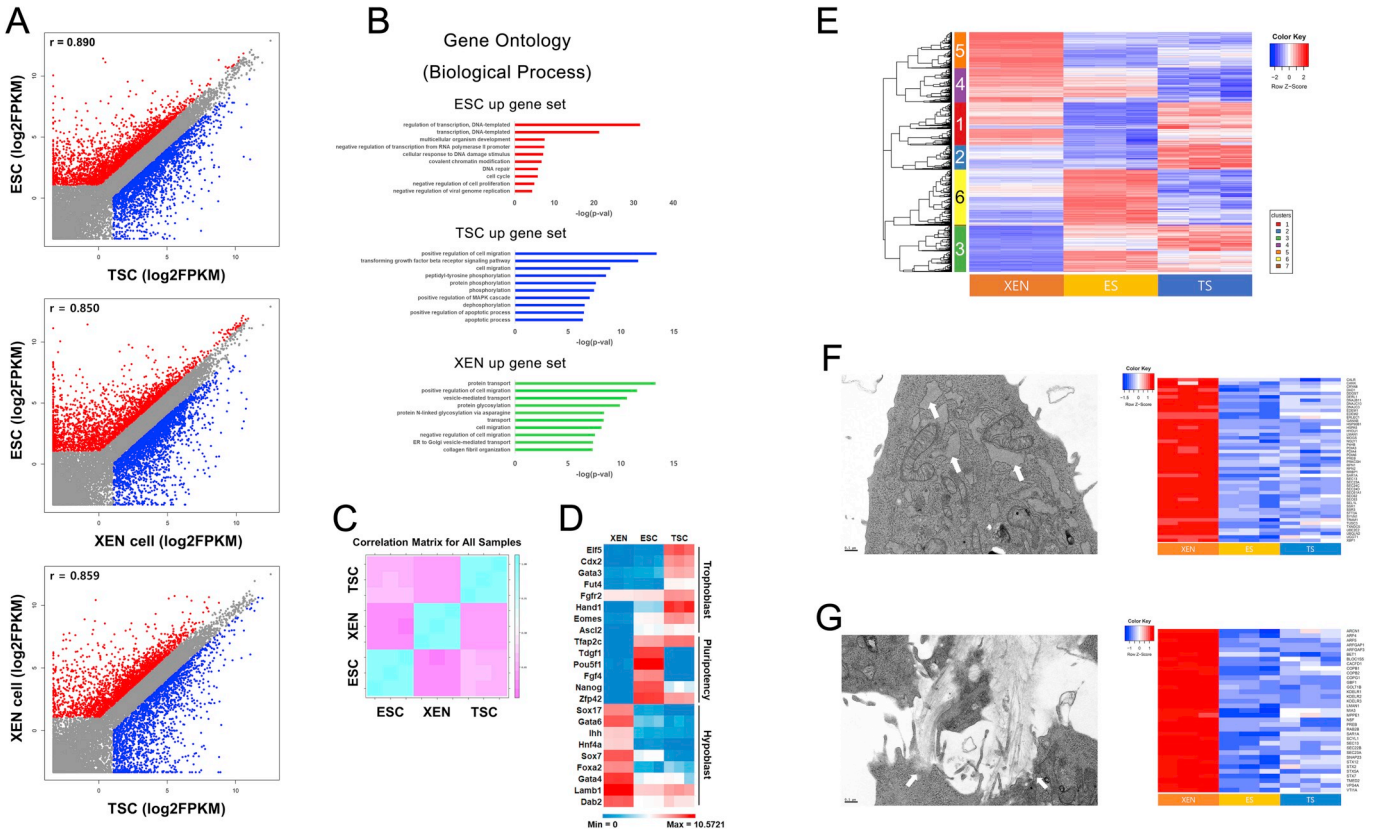

Fig. 5. RNA sequencing analysis of ESC, TSC, and XEN cells. **(A)** Scatterplot analysis of ESCs, TSCs, and XEN cells. **(B)** GO:BP analysis of enriched genes among the DEGs in ESCs, TSCs, and XEN cells. **(C)** Correlation matrix analysis of ESCs, TSCs, and XEN cells. **(D)** Heatmap of lineage-specific gene expression in ESCs, TSCs, and XEN cells. **(E)** Heatmap clusters of DEGs between ESCs, TSCs, and XEN cells. **(F)** Enlarged TEM image of swollen endoplasmic reticulum (white arrows) in XEN cell. Heatmap analyses confirmed that gene sets involved in 'protein processing in ER' were dramatically upregulated in XEN cells compared with that in ESCs and TSCs. Scale bar: 0.5 μm **(G)** Enlarged TEM image of XEN cell spurting proteins. Heatmap analyses confirmed that gene sets involved in 'vesicle-mediated transport' were dramatically upregulated in XEN cells compared with that in ESCs and TSCs. Scale bar: 0.5 μm. ESC, embryonic stem cells; TSC, trophoblast stem cells; XEN, extraembryonic endoderm.

cell surface and ERs of XEN cells by TEM analysis (Fig. 5F and 5G). XEN cells showed swollen form of ERs (Fig. 5F, left), which is commonly observed in secretory cell types. In addition, many spurting bodies were observed on the surface of XEN cells (Fig. 5G, left). Heatmap analyses confirmed that gene sets involved in 'vesicle-mediated transport' and 'protein processing in ER' were dramatically upregulated in XEN cells compared with that in ESCs and TSCs (Fig. 5F-G, right).

4. Discussion

In this study, we first compared the mitochondrial morphology and energy metabolism of three different types of stem cells (ESCs, TSCs, and XEN cells) that were derived from blastocysts. The newly established ESCs, TSCs, and XEN cells were compared based on electron microscopy analysis, energy metabolic analysis, and gene expression profiling via RNA sequencing. Consistent with previous reports, our results showed that pluripotent ESCs contained immature mitochondria with fewer cristae. Interestingly, the TE cell-derived multipotent TSCs also showed similar mitochondrial morphology as the ESCs. Initially, we predicted that ESCs would be closer to XEN cells than to TSCs, since ICM and TE separate at 3.5 dpc and epiblast and PrE separate from the same origin (ICM) at 4.5 dpc. However, contrary to our expectation, the ESCs and TSCs showed similar mitochondrial morphology and energy metabolism, while the ICM-derived cells, ESCs and XEN cells showed more differences than that between ESCs and TSCs.

According to the electron microscopic observations, XEN cells displayed relatively mature form of mitochondria compared to that in ESCs and TSCs. The mature form of mitochondria, which have complex cristae structure, are thought to produce energy more efficiently than the immature form, because they have a larger amount of inter-membrane proteins for energy production in the complex cristae [19]. We analyzed OCR for determining the metabolic capacity such as basal respiration, ATP production, maximal respiration, and spare respiratory capacity. Usually, somatic cells, which perform cell-specific function, require more energy than stem cells whose main function is maintaining stem cell state by self-renewal. Interestingly, among the three cell types, ESCs produced more energy than the other two stem cell types. Although there is no clear explanation for this phenomenon, the higher proliferation rate of ESCs compared with that of TSCs and XEN cells (Fig. 1C) might affect the energy demands, leading to higher ATP production; as highly proliferative cells, the ESCs may need more metabolic compounds for cell division [20,21]. Pala et al. showed that more proliferative cells produce more energy than quiescent cells, indicating the dynamics of metabolic requirements according to the cell state [22]. However, another report suggested that the quiescent state does not necessarily entail reduced metabolic activity [23]. Thus, ATP production level may reflect the cell type specificity as well as cell proliferation rate.

Another intriguing finding was that XEN cells contained swollen form of ER and overexpressed gene sets involved in 'protein processing in ER' and 'ER to Golgi vesicle-mediated transport', compared with that in ESCs and TSCs. The swollen form of ERs are commonly observed in secretory cell types [24], and ER to Golgi transport is part of biosynthetic secretory pathways [25,26]. Therefore, it is speculated that the secretion pathway or cell-cell communication through protein transport may be active processes in XEN cells; it will be very interesting to

investigate the cell-cell communication mechanism in XEN cells in future.

In the present study, we showed that ICM and TE showed similar mitochondrial morphology and their derivatives, namely ESCs and TSCs, also showed indistinguishable morphology of mitochondria (Fig. 3B and Supplementary Figs. 2E–H). We could not compare the morphology of epiblast and PrE, as it was very difficult to discriminate between them using transmission electron microscopy. However, we speculate that the PrE cells might contain similar form of mitochondria as observed in XEN cells, because similar mitochondrial morphology was observed between ICM and ESCs, and TE and TSCs. However, we cannot guarantee that the metabolic and mitochondrial data obtained from *in vitro* cultured stem cells represent the state of epiblast, PrE, and TE cells of blastocyst that are developing *in vivo*. The three cell types of blastocyst are not in stem cell state, but rather in the middle of differentiation into respective lineages. The culture conditions also differ; epiblast, PrE, and TE cells are maintained in the same environment, while ESCs, TSCs, and XEN cells are maintained in their own special medium containing cell type-specific self-renewal signaling molecules [27,28]. Thus, the precise energy metabolism in epiblast, PrE, and TE cells of blastocyst should be measured using separated cells from the blastocyst. In addition, because the level of oxygen in the uterus of mouse is as low as 3.5–5% during the peri-implantation stage [29], hypoxic culture condition is required to simulate the *in vivo* state of blastocysts. Human ESCs, which largely depend on glycolysis for ATP production, activate the OXPHOS system when cultured in a medium with lipid supplements [30]. Taken together, the cellular environment could be a key factor influencing the mitochondrial morphology and energy metabolism.

Our data also showed that TSCs containing immature form of mitochondria like ESCs showed the lowest basal and maximal respiration. This result indicates that although the mitochondrial morphologies of ESC and TSC are similar, their energy metabolism might differ depending on the cell type. XEN cells showed relatively much higher spare respiratory capacity, which may be linked to the complex cristae, where a larger number of proteins related to the electron transport chain exist [31,32]. In contrast to the TSCs, the spare respiratory capacity of the ESCs was almost zero, indicating that ESCs are more dependent on glycolysis than TSCs, although TSCs showed a higher activity of glycolytic functions. The exact mechanism underlying the higher dependence of ESCs on aerobic glycolysis than that of the TSCs remains elusive. Higher levels of ATP in TSCs might be a result of the process of glycolysis because the ATP-linked respiration in ESCs and TSCs are not much different (Fig. 4E). This phenomenon was also observed in many cancer cells and is known as aerobic glycolysis or the Warburg effect [13]. Aerobic glycolysis in cancer cells was suggested to be associated with a tendency to create an immunosuppressive environment that promotes cell survival and growth. However, it is not yet certain whether the ESCs, TSCs, and cancer cells utilize aerobic glycolysis for similar purposes. If yes, then the study on ESC and TSC metabolism could be applied to understand and control cancer metabolism. Aerobic glycolysis may be advantageous for the unlimited self-renewal ability, which is a common feature between pluripotent stem cells and cancer cells.

In this study, we clearly showed that blastocyst-derived stem cells have various morphologies of mitochondria linked to metabolic characteristics. In addition, the analysis of OCR and ECAR could prove helpful in understanding the overall metabolic machinery in detail. Our analysis allows us to understand the mechanism of the first differentiation of the embryo and the associated dynamic changes in metabolism.

Recently, Zernicka-goetz et al. reported synthetic embryo [33]; the ETX embryoid could be formed by assembling the three types of stem cells, namely ESC, TSC, and XEN cell. However, the underlying mechanism of this assembly and the effect of each cell type on the others were not verified in detail. We propose that analysis of the unveiled energy metabolism of the three cell types could provide mechanistic insights into the metabolism of the self-assembled ETX embryoid.

Declaration of competing interest

The authors declare that they have no conflicts of interest.

Acknowledgments

This research was supported by the Basic Science Research Program through the National Research Foundation of Korea (NRF) funded by the Ministry of Science, ICT and Future Planning of the Republic of Korea (grant nos. 2016M3A9B6946835 and 2015R15A1009701).

Appendix A. Supplementary data

Supplementary data to this article can be found online at https://doi.org/10.1016/j.redox.2020.101437.

Author contribution statement

BJS, JC and JTD wrote the main manuscript text and designed the study. BJS, JC, HL, SHY and JHL performed experiments and analyzed the data. BJS, KH, JHL, HMC, and JTD performed data analysis. All authors reviewed the manuscript.

References

[1] J. Artus, C. Chazaud, A close look at the mammalian blastocyst: epiblast and primitive endoderm formation, Cell. Mol. Life Sci. 71 (17) (2014) 3327–3338.
[2] V. Bryja, S. Bonilla, E. Arenas, Derivation of mouse embryonic stem cells, Nat. Protoc. 1 (4) (2006) 2082–2087 PubMed PMID: 17487198.
[3] K.K. Niakan, N. Schrode, L.T. Cho, A.K. Hadjantonakis, Derivation of extra-embryonic endoderm stem (XEN) cells from mouse embryos and embryonic stem cells, Nat. Protoc. 8 (6) (2013 Jun) 1028–1041 PubMed PMID: 23640167. Pubmed Central PMCID: 3927835.
[4] S. Tanaka, T. Kunath, A.-K. Hadjantonakis, A. Nagy, J. Rossant, Promotion of trophoblast stem cell proliferation by FGF4, Science 282 (5396) (1998) 2072–2075.
[5] M.J. Evans, M.H. Kaufman, Establishment in culture of pluripotential cells from mouse embryos, Nature 292 (5819) (1981) 154.
[6] T. Kunath, D. Arnaud, G.D. Uy, I. Okamoto, C. Chureau, Y. Yamanaka, et al., Imprinted X-inactivation in extra-embryonic endoderm cell lines from mouse blastocysts, Development 132 (7) (2005) 1649–1661.
[7] G.M. Kelly, M.I. Gatie, Mechanisms regulating stemness and differentiation in embryonal carcinoma cells, Stem Cell. Int. 2017 (2017).
[8] C. Hu, L. Fan, P. Cen, E. Chen, Z. Jiang, L. Li, Energy metabolism plays a critical role in stem cell maintenance and differentiation, Int. J. Mol. Sci. 17 (2) (2016) 253.
[9] M. Zick, R. Rabl, A.S. Reichert, Cristae formation—linking ultrastructure and function of mitochondria, Biochim. Biophys. Acta Mol. Cell Res. 1793 (1) (2009) 5–19.
[10] R. Rossignol, R. Gilkerson, R. Aggeler, K. Yamagata, S.J. Remington, R.A. Capaldi, Energy substrate modulates mitochondrial structure and oxidative capacity in cancer cells, Cancer Res. 64 (3) (2004) 985–993.
[11] W. Zhou, M. Choi, D. Margineantu, L. Margaretha, J. Hesson, C. Cavanaugh, et al., HIF1α induced switch from bivalent to exclusively glycolytic metabolism during ESC-to-EpiSC/hESC transition, EMBO J. 31 (9) (2012) 2103–2116.
[12] O. Warburg, On the origin of cancer cells, Science 123 (3191) (1956) 309–314.
[13] M.V. Liberti, J.W. Locasale, The Warburg effect: how does it benefit cancer cells? Trends Biochem. Sci. 41 (3) (2016) 211–218.
[14] M.D. Buck, D. O'Sullivan, R.I.K. Geltink, J.D. Curtis, C.-H. Chang, D.E. Sanin, et al., Mitochondrial dynamics controls T cell fate through metabolic programming, Cell 166 (1) (2016) 63–76.
[15] H.W. Choi, J.H. Kim, M.K. Chung, Y.J. Hong, H.S. Jang, B.J. Seo, et al., Mitochondrial and metabolic remodeling during reprogramming and differentiation of the reprogrammed cells, Stem Cells Dev. 24 (11) (2015) 1366–1373.
[16] V.A. Rafalski, E. Mancini, A. Brunet, Energy metabolism and energy-sensing pathways in mammalian embryonic and adult stem cell fate, J. Cell Sci. 125 (23) (2012) 5597–5608.
[17] J. Rossant, Mouse and human blastocyst-derived stem cells: vive les differences, Development 142 (1) (2015 Jan 1) 9–12 PubMed PMID: 25516964.
[18] H.W. Choi, J.Y. Joo, Y.J. Hong, J.S. Kim, H. Song, J.W. Lee, et al., Distinct enhancer activity of Oct4 in naive and primed mouse pluripotency, Stem Cell Rep. 7 (5) (2016) 911–926.
[19] M. Zick, R. Rabl, A.S. Reichert, Cristae formation-linking ultrastructure and function of mitochondria, Biochim. Biophys. Acta 1793 (1) (2009 Jan) 5–19 PubMed PMID: 18620004.
[20] Metabolic pathway alterations that support cell proliferation, in: M. Vander Heiden,

S. Lunt, T. Dayton, B. Fiske, W. Israelsen, K. Mattaini, et al. (Eds.), Cold Spring Harbor Symposia on Quantitative Biology, Cold Spring Harbor Laboratory Press, 2011.
[21] B. Seo, S. Yoon, J. Do, Mitochondrial dynamics in stem cells and differentiation, Int. J. Mol. Sci. 19 (12) (2018) 3893.
[22] F. Pala, D. Di Girolamo, S. Mella, S. Yennek, L. Chatre, M. Ricchetti, et al., Distinct metabolic states govern skeletal muscle stem cell fates during prenatal and postnatal myogenesis, J. Cell Sci. 131 (14) (2018) jcs212977.
[23] J.M. Lemons, X.-J. Feng, B.D. Bennett, A. Legesse-Miller, E.L. Johnson, I. Raitman, et al., Quiescent fibroblasts exhibit high metabolic activity, PLoS Biol. 8 (10) (2010) e1000514.
[24] Y. Sakai, S. Yamashina, S.I. Furudate, Missing Secretory Granules, Dilated Endoplasmic Reticulum, and Nuclear Dislocation in the Thyroid Gland of Rdw Rats with Hereditary Dwarfism vol. 259, The Anatomical Record: An Official Publication of the American Association of Anatomists, 2000, pp. 60–66 (1).
[25] J.M. Herrmann, A. Spang, Intracellular Parcel Service: Current Issues in Intracellular Membrane Trafficking. Membrane Trafficking, Springer, 2015, pp. 1–12.
[26] G. Jalagadugula, L.E. Goldfinger, G. Mao, M.P. Lambert, A.K. Rao, Defective RAB1B-related megakaryocytic ER-to-Golgi transport in RUNX1 haplodeficiency: impact on von Willebrand factor, Blood Adv. 2 (7) (2018) 797–806.
[27] Y. Zhong, B. Binas, Transcriptome analysis shows ambiguous phenotypes of murine primitive endoderm-related stem cell lines, Genes Cells 24 (4) (2019) 324–331.
[28] D. Li, J. Liu, X. Yang, C. Zhou, J. Guo, C. Wu, et al., Chromatin accessibility dynamics during iPSC reprogramming, Cell Stem Cell 21 (6) (2017) 819–833 e6.
[29] B. Fischer, B. Bavister, Oxygen tension in the oviduct and uterus of rhesus monkeys, hamsters and rabbits, Reproduction 99 (2) (1993) 673–679.
[30] H. Zhang, M.G. Badur, A.S. Divakaruni, S.J. Parker, C. Jäger, K. Hiller, et al., Distinct metabolic states can support self-renewal and lipogenesis in human pluripotent stem cells under different culture conditions, Cell Rep. 16 (6) (2016) 1536–1547.
[31] B.G. Hill, B.P. Dranka, L. Zou, J.C. Chatham, V.M. Darley-Usmar, Importance of the bioenergetic reserve capacity in response to cardiomyocyte stress induced by 4-hydroxynonenal, Biochem. J. 424 (1) (2009) 99–107.
[32] H. Yamamoto, K. Morino, L. Mengistu, T. Ishibashi, K. Kiriyama, T. Ikami, et al., Amla Enhances Mitochondrial Spare Respiratory Capacity by Increasing Mitochondrial Biogenesis and Antioxidant Systems in a Murine Skeletal Muscle Cell Line. Oxidative Medicine and Cellular Longevity, (2016) 2016.
[33] S.E. Harrison, B. Sozen, N. Christodoulou, C. Kyprianou, M. Zernicka-Goetz, Assembly of embryonic and extraembryonic stem cells to mimic embryogenesis in vitro, Science 356 (6334) (2017) eaal1810.